

## HIGH RESOLUTION X-RAY SPECTROSCOPY OF THE FE K COMPLEX IN IC 4329A

BARRY MCKERNAN<sup>1,2</sup> AND TAHIR YAQOOB<sup>2,3</sup>  
*Draft version October 30, 2018*

### ABSTRACT

We report the detection of complex Fe K line emission from a *Chandra* High Energy Transmission Grating Spectrometer (*HETGS*) observation of the Seyfert 1 galaxy IC 4329A. The line emission is double-peaked, one peak centered at  $\sim 6.3$  keV, and the other at  $\sim 6.9$  keV in the source rest frame. When modeled by Gaussians, the lower energy peak is resolved by the HEG at  $> 99\%$  confidence, whilst the higher energy peak is resolved at only  $< 90\%$  confidence. The best-fitting widths are  $\sim 21,000$  km s<sup>-1</sup> and  $\sim 4000$  km s<sup>-1</sup> FWHM for the  $\sim 6.3$  keV and  $\sim 6.9$  keV peaks respectively. If the peaks correspond to two distinct emission lines, then the peak energies are redshifted with respect to the expected line energies of Fe I K $\alpha$  and Fe XXVI Ly $\alpha$  by at least 650 km s<sup>-1</sup> and 950 km s<sup>-1</sup> respectively. Alternatively, the Fe K line profile may be due to a single line from a relativistic accretion disk. In that case the inclination angle of the disk is required to be  $24_{-1}^{+9}$  degrees, the outer radius constrained to several tens of gravitational radii, and the radial line emissivity flatter than  $r^{-0.7}$ . Another possibility is that both peaks are due to distinct lines but each one relativistically broadened by a disk. In that case the lower energy peak could correspond to emission from Fe in a low ionization state, and the high-energy peak to Fe XXVI Ly $\alpha$  emission. Then, the inclination angle is even less, restricted to a few degrees. However, the radial emissivity law is allowed to be steeper ( $\sim r^{-2.5}$ ) and the outer radius does not have to be fine-tuned. Yet another scenario is that the lower energy peak originates in a disk but the higher energy peak originates in more distant matter. The disk inclination angle is then intermediate between the last two cases but the emissivity is again required to be flat. We cannot rule out Fe XXV He-like absorption modifying the observed line profile. However, the data, and inferred emission-line parameters, are insensitive to the presence of a Compton reflection continuum. Including Compton reflection does, however, allow a steeper radial emissivity law for the relativistic line. Future missions such as *Astro-E2* will be able to break a lot of the degeneracy in the physically distinct models that can all account for the *Chandra* data. Since IC 4329A is one of the brightest Seyfert 1 galaxies it should be a good astrophysical laboratory for studying the ionization structure of accretion disks around supermassive black holes.

*Subject headings:* galaxies: active – galaxies: individual (IC 4329A) – galaxies: Seyfert – techniques: spectroscopic – X-rays: line – emission: accretion – disks: galaxies

### 1. INTRODUCTION

Some of the Fe K $\alpha$  fluorescent emission line in active galactic nuclei (AGNs) is believed to originate in a relativistic accretion disk around a supermassive black hole (see e.g. reviews by Fabian *et al.* 2000; Reynolds & Nowak 2003). Early studies of type 1 AGN using X-ray observations with ASCA revealed a wide variety of Fe K $\alpha$  line widths and shapes (e.g. Nandra *et al.* 1997; Lubiński, P. & Zdziarski 2001; Perola *et al.* 2002; Yaqoob *et al.* 2002). These results have been confirmed with the advent of the *Chandra* and *XMM-Newton* X-ray observatories, but a more complex picture is emerging. New, high resolution observations are revealing that a narrow Fe K line ( $< 10,000$  km s<sup>-1</sup> FWHM) component is common in type 1 AGN (Yaqoob *et al.* 2001; Kaspi *et al.* 2002; Pounds *et al.* 2001; Turner *et al.* 2002; Fang *et al.* 2002; Reeves *et al.* 2002; Yaqoob & Padmanabhan 2004), often superimposed on top of a broad ( $\sim 10,000$ – $100,000$  km s<sup>-1</sup> FWHM) component. Traditionally, narrow Fe K lines are associated with matter at least several thousand gravitational radii from the black hole (one gravitational radius,  $r_g$ , defined as  $GM/c^2$ ). However, there is increasing evidence to suggest that narrow

Fe K lines can originate in, or have a significant contribution from, the putative accretion disk (Petrucci *et al.* 2002; Lee *et al.* 2002; Yaqoob *et al.* 2003a). Narrow Fe K lines originating from a disk can be interpreted in terms of truncated disk emission (e.g. Done, Madejski, & Życki 2000) or in terms of a flattened radial line emissivity where the intensity per unit area falls off less steeply than  $\sim r^{-2}$  (Yaqoob *et al.* 2003a). Alternatively, the narrow Fe K lines could be due to localized emission from the disk (Turner *et al.* 2002; Yaqoob *et al.* 2003a). There are, of course, other possible interpretations of the origin of narrow Fe K lines (e.g. Sulentic *et al.* 1998; Elvis 2000; Hartnoll & Blackman 2000).

Earlier observations with ASCA also identified Fe K-shell emission due to highly ionized (H-like) Fe in two type 1 AGN, PG 1116+215 (Nandra *et al.* 1996) and Ton S 180 (Turner *et al.* 1998; Comastri *et al.* 1998). Observations with the *Chandra* high energy transmission grating spectrometer (*HETGS*) and the *XMM-Newton* CCD detectors are now revealing Fe K emission due to H-like and He-like Fe in other AGN (e.g. Reeves *et al.* 2002; Dewangan 2002; Page, Davis, & Salvi 2003; Yaqoob *et al.* 2003a). As more examples of highly ionized Fe spectral features are detected in the spectra of type 1 AGN, it is clear that we need a better understanding of the complex ionization physics of the accretion disk (e.g. Nayakshin & Kallman 2001; Ballantyne, Ross & Fabian 2001; Ballantyne & Ross 2002).

Here we report on the spectral results of a *Chandra HETGS* observation of the type 1 AGN IC 4329A, in which we ob-

<sup>1</sup> Present Address: Department of Astronomy, University of Maryland, College Park, MD 20742

<sup>2</sup> Department of Physics and Astronomy, Johns Hopkins University, Baltimore, MD 21218

<sup>3</sup> Laboratory for High Energy Astrophysics, NASA/Goddard Space Flight Center, Greenbelt, MD 20771

serve a complex, broad, double-peaked line profile. Preliminary results of this observation were presented in Yaqoob & Padmanabhan (2004) and we now present detailed modeling of the Fe K line profile at the highest spectral resolution yet available (FWHM  $\sim 1860$  km s $^{-1}$  at 6.4 keV). IC 4329A is a bright Seyfert 1.2 AGN at  $z = 0.016054$  (Willmer *et al.* 1991) embedded in a nearly edge-on host galaxy. It is one of the brightest Seyfert galaxies known, and is sometimes brighter than 3C 273 in the 2–10 keV band. IC 4329A is luminous, with  $L$  (2–10 keV)  $\sim 4 \times 10^{43}$  ergs s $^{-1}$  typically, where we have converted from the luminosity given by Reynolds (1997) using  $H_0 = 71$  km s $^{-1}$ Mpc $^{-1}$  (Spergel *et al.* 2003) and  $q_0 = 0$ .

IC 4329A was observed previously with *ASCA* (Mushotzky *et al.* 1995; Cappi *et al.* 1996), *GRO* (Madejski *et al.* 1995), *BeppoSAX* (Perola *et al.* 1999), *ASCA* simultaneously with *RXTE* (Done, Madejski & Życki 2000) and *XMM-Newton* simultaneously with *BeppoSAX* (Gondoin *et al.* 2001). A Gaussian model fitted to the *ASCA* observations (Done, Madejski & Życki 2000) revealed strong (EW =  $180 \pm 50$  keV), broad (FWHM =  $42,960 \pm 11,015$  km s $^{-1}$ ) Fe K emission peaking near  $\sim 6.4$  keV. The *XMM-Newton* observations (Gondoin *et al.* 2001) revealed a narrow Fe K $\alpha$  line (FWHM  $< 8785$  km s $^{-1}$ , EW =  $43 \pm 1$  eV) originating in matter with a low ionization state (the line peaked at  $E = 6.42^{+0.04}_{-0.03}$  keV).

The paper is organized as follows. In §2 we discuss the observation and data. In §3 we discuss fitting different physical models of the complex spectrum in the Fe K band. In §4 we discuss the implications of our results and present our conclusions.

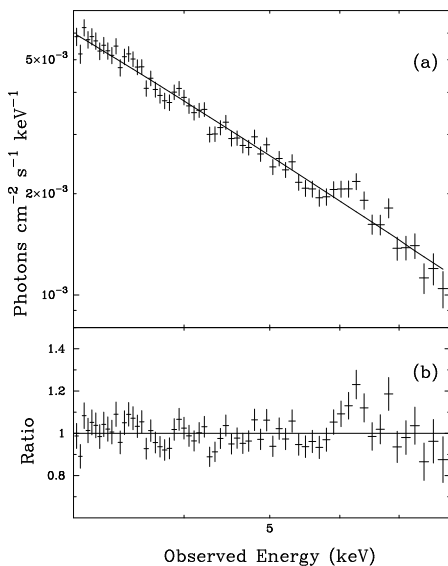


FIG. 1.— IC 4329A HEG spectrum between 3.0 and 8.0 keV binned at  $0.16\text{\AA}$  compared with the best-fitting power-law model. (a) Photon spectrum, (b) Ratio of the data to the model.

## 2. OBSERVATION AND DATA

IC 4329A was observed with the *Chandra HETGS* (Markert *et al.* 1995) on 2001 August 26 from UT 06:14:07 for a duration of  $\sim 60$  ks. The *Chandra HETGS* consists of two grating assemblies, a high-energy grating (HEG) and a medium-energy grating (MEG). We used only the combined  $\pm 1$  orders of the grating data. The mean *Chandra* total HEG and MEG count rates were  $1.158 \pm 0.0051$  ct/s and  $2.244 \pm 0.0067$  ct/s respectively. The source flux showed little variability over the

entire duration of the campaign. For example, for HEG plus MEG combined first-order lightcurves binned at 128 s, the excess variance above the expectation for Poisson noise (e.g. see Turner *et al.* 1999) was  $(3.4 \pm 18.2) \times 10^{-5}$ , consistent with zero. Only single spectra per instrument were therefore extracted.

We made effective area files (ARFs or *ancillary response files*), photon spectra and counts spectra following the method of Yaqoob *et al.* (2003b). A net exposure time of 59,087 s was obtained (including a deadtime factor of 0.0162). The HEG bandpass is  $\sim 0.8$ –10 keV and the MEG bandpass is  $\sim 0.5$ –10 keV but the effective area of both instruments falls off rapidly at either end of the bandpass. Background was not subtracted since it is negligible in the energy region of interest. The HEG has twice the spectral resolution ( $0.012\text{\AA}$  FWHM) of the MEG ( $0.023\text{\AA}$  FWHM) and has a larger effective area than the MEG in the Fe K band so our analysis will focus on the HEG data, since we are interested in studying the Fe K region with the highest spectral resolution currently available. The MEG spectrum of IC 4329A is discussed elsewhere (McKernan, Yaqoob, & Reynolds 2004, in preparation).

## 3. MODELING OF THE FE K COMPLEX IN IC 4329A

We used XSPEC v.11.2.0 for spectral fitting to the HEG spectrum in the 3–8 keV band. This choice for the lower end of the bandpass avoids the known complexities in the soft X-ray spectrum due to absorption and the higher end ensures that background will indeed be negligible since the instrument efficiency area vanishes rapidly at high energies. Galactic absorption of  $4.55 \times 10^{20}$  cm $^{-2}$  (Elvis *et al.* 1989) has a negligible effect in this energy range and so was not included in our modeling. There has been a well-documented degradation in the quantum efficiency of *Chandra* ACIS due to molecular contamination. However, the effect of this degradation is most pronounced at energies below  $\sim 1$  keV and is negligible over the energy range discussed here so we do not include ACIS degradation in our modeling. The  $C$ -statistic (Cash 1976) was used for minimization in all models and all statistical errors quoted are 90% confidence for one interesting parameter ( $\Delta C = 2.706$ ), unless otherwise stated.

First we investigated how the 3.0–8.0 keV HEG data compared with a simple model consisting of a single power law plus intrinsic absorption, with the spectrum binned at  $0.16\text{\AA}$ . We included absorption in this initial fit, just to ensure that it can be neglected in the bandpass that we used. The best-fitting power-law index for this model was  $1.66^{+0.09}_{-0.05}$  and the absorbing column density was zero with an upper limit of  $5.1 \times 10^{21}$  cm $^{-2}$ . Figure 1(a) shows the HEG photon spectrum of IC 4329A with the model superimposed. Figure 1(b) shows the ratio of the data to the model. The single power law is clearly a good overall fit to the hard X-ray spectrum but there is a broad double-peaked feature in the Fe K band. The peaks occur at  $\sim 6.2$  keV and  $\sim 6.8$  keV in the observed frame, and the lower energy feature appears to be broader than the high-energy one. To investigate the Fe-K emission complex in more detail, we used spectra binned at  $0.005\text{\AA}$ , which corresponds approximately to the  $1\sigma$  HEG resolution. Since no absorption is required in the 3–8 keV band, we used only a power law for the continuum. Several models of the complex Fe K emission are discussed below.

### 3.1. Double Gaussian Model

We added two Gaussian emission-line components to the power-law continuum model in order to fit the  $\sim 6.2$  keV and  $\sim 6.8$  keV emission peaks. We did not include a Compton reflection continuum in the fit since we will show *post-facto* that the emission-line parameters are insensitive to the presence or absence of a Compton reflection continuum (see §3.6). The best-fitting parameters for this model are given in Table 1. Note that in Table 1 we show the velocity shift from systemic when the lower and higher-energy peaks are identified with Fe I  $K\alpha$  emission (at 6.400 keV in the rest frame) and H-like Fe XXVI  $Ly\alpha$  emission (at 6.966 keV rest frame) respectively. Even when we take into account the systematic uncertainty of the HEG wavelength scale ( $\sim \pm 420, \pm 460$  km s $^{-1}$  at  $\sim 6.2$  keV and  $\sim 6.8$  keV respectively)<sup>4</sup>, the low-energy feature (if Fe I  $K\alpha$  emission) is redshifted by  $> 650$  km s $^{-1}$  and the higher energy feature (if Fe XXVI  $Ly\alpha$ ) is redshifted by  $> 950$  km s $^{-1}$  (both are 90% confidence lower limits). If the higher energy feature is due to Fe XXV forbidden or Fe XXV resonance emission, then the blueshift is  $\sim 12,200$  km s $^{-1}$  or  $\sim 9,220$  km s $^{-1}$  respectively, relative to systemic velocity.

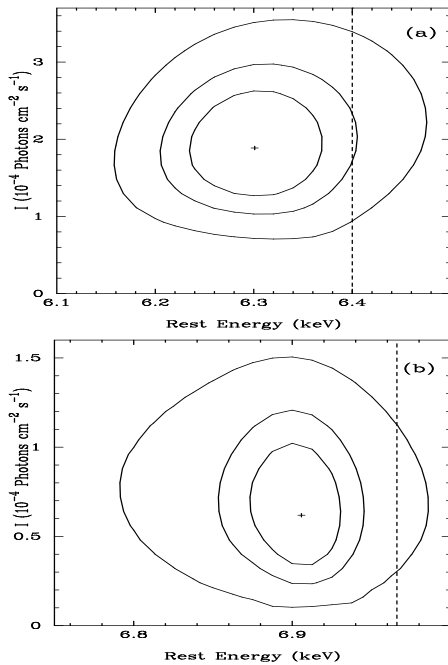


FIG. 2.— Confidence contours of line intensity versus rest-frame energy for (a) the lower energy Fe K peak and (b) the higher energy peak from a double Gaussian model fit to the HEG spectrum of IC 4329A (see §3.1 and Table 1). The two-parameter joint confidence levels correspond to 68%, 90%, and 99% confidence. The dashed line in (a) denotes the rest-frame energy for Fe I  $K\alpha$  emission (6.400 keV) and that in (b) corresponds to the rest-energy of Fe XXVI  $Ly\alpha$  emission (6.966 keV). The contours in (a) indicate that the lower energy feature is redshifted from the Fe I  $K\alpha$  rest-energy at  $\sim 90\%$  confidence. From (b) it appears that the higher energy feature is redshifted from the rest-energy of the Fe XXVI  $Ly\alpha$  emission line.

The low-energy Fe K feature is moderately broad (FWHM= $20,825^{+10,110}_{-7375}$  km s $^{-1}$ ), as we saw from Fig. 1, whereas the higher energy feature is narrower (FWHM= $3680^{+5200}_{-2455}$  km s $^{-1}$ ). We estimated the significance of each feature by comparing the values of the  $C$ -statistic obtained from fitting a power-law continuum only and from adding the feature in question to the power-law only fit. The resulting values of  $\Delta C$  are shown in Table 1. The addition

of each Gaussian component adds three free parameters to a fit, so the lower energy Fe K feature was detected with a confidence level  $> 4\sigma$  and the higher energy feature was detected at only  $> 95\%$  confidence.

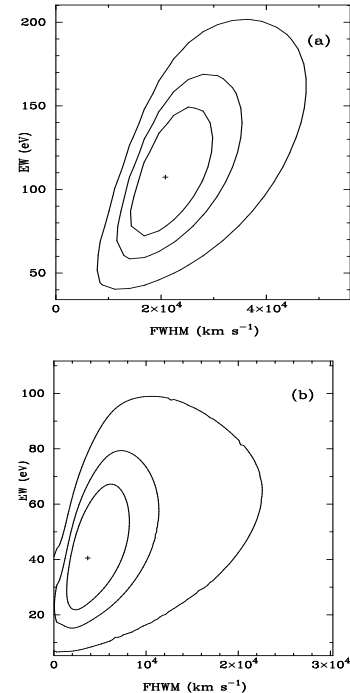


FIG. 3.— Confidence contours of equivalent width (EW) versus FWHM for (a) the lower energy Fe K emission peak and (b) the higher energy peak from a double-Gaussian model fit to the HEG spectrum of IC 4329A (see §3.1 and Table 1). The two-parameter joint confidence levels correspond to 68% (innermost), 90% and 99% (outermost).

Fig. 2(a) shows a two-parameter joint confidence contour of line intensity versus rest-frame energy for the lower energy Fe K emission and Fig. 2(b) shows a similar plot for the higher energy emission. Consistent with the spectral fitting results, it can be seen that the lower energy Fe K emission peak is marginally redshifted from the rest-frame energy of Fe I  $K\alpha$  (dashed line) at  $\sim 90\%$  confidence. If we identify the higher energy feature with Fe XXVI  $Ly\alpha$  emission, this line is also marginally (at  $> 90\%$  confidence) redshifted with respect to systemic velocity (dashed line). Fig. 3(a) shows a two-parameter joint confidence contour of the equivalent width (EW) versus FWHM for the lower energy Fe K emission and Fig. 3(b) shows a similar plot for the higher energy emission peak.

Fig. 4(a) shows a close-up of the best-fitting Gaussian model fit (see Table 1) to the IC 4329A HEG spectrum. Again, the offset of the Gaussian peak energies from the dashed lines in Fig. 4(a), which mark the energies of Fe I  $K\alpha$  and Fe XXVI  $Ly\alpha$  emission in the observed frame (6.299 keV and 6.856 keV respectively), show that both the lower and higher energy peaks (if Fe I  $K\alpha$  and Fe XXVI  $Ly\alpha$  respectively) are indeed marginally redshifted in IC 4329A. If the higher energy feature is Fe XXVI  $Ly\alpha$  emission, then under some circumstances we should also expect significant Fe XXVI  $Ly\beta$  emission (e.g. see Bautista *et al.* 1998; Bautista & Titarchuk 1999). We therefore added a third Gaussian component to the model in Table 1 and we extended the HEG data energy range to 3.0–8.3 keV since Fe XXVI  $Ly\beta$  occurs at 8.251 keV in the rest-frame (for all successive mod-

<sup>4</sup> <http://space.mit.edu/CXC/calib/hetgcal.html>

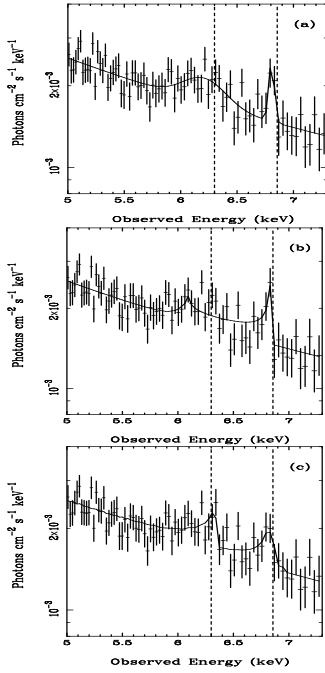


FIG. 4.— IC 4329A HEG photon spectra between 5.0 and 7.3 keV (observed energy), binned at  $0.01\text{\AA}$ . The solid lines correspond to physically different (and degenerate) models (see text for details). Note that the data are *not* unfolded: the spectra were made by multiplying the ratio of the counts in each spectral bin to the predicted model counts in that bin, by the best-fitting model. In each case the continuum is a simple power law and the emission-line models are (a) a double Gaussian (see §3.1 and Table 1); (b) a single disk line (see §3.2 and Table 2), and (c) a double disk line (see §3.4 and Table 3). Dashed lines indicate the observed-frame energies expected for Fe I  $K\alpha$  (6.400 keV) and Fe XXVI  $\text{Ly}\alpha$  (6.966 keV) emission respectively.

els we shall return to fitting the data range 3.0–8.0 keV). Fe XXVI  $\text{Ly}\beta$  is hardly detected ( $\Delta C$  improves by only  $\sim 1$  for the addition of a Gaussian with three free parameters, and  $\text{EW} < 49\text{eV}$ ). The value of the Fe  $\text{Ly}\beta$ : $\text{Ly}\alpha$  ratio is a powerful diagnostic since it can determine the process of excitation. However, the measurement errors on the Fe  $\text{Ly}\beta$ : $\text{Ly}\alpha$  ratio in these data are too large to obtain any meaningful constraints. On the other hand, since IC 4329A is one of the brightest Seyfert galaxies (sometimes it is brighter than 3C 273), it is one of the best candidates to constrain the Fe  $\text{Ly}\beta$ : $\text{Ly}\alpha$  ratio with future missions such as *Astro-E2*. We obtained the observed-frame 2–10 keV flux (for comparison with values in the literature) for the *Chandra* HEG spectrum by extrapolating the above best-fitting model down to 2 keV and up to 10 keV, and this yielded a value of  $16.2 \times 10^{-11} \text{ erg cm}^{-2} \text{ s}^{-1}$ , corresponding to an intrinsic, source-frame 2–10 keV luminosity of  $9 \times 10^{43} \text{ erg s}^{-1}$ .

Since we detected an emission line peak that could be due to Fe XXVI  $\text{Ly}\alpha$  we searched for evidence of other features due to highly ionized Fe (as detected e.g. in NGC 7314 by Yaqoob *et al.* 2003a) by adding a third Gaussian model component. We find  $\text{EW} < 17\text{eV}$  for Fe XXV (f) (at the same offset velocity and the width of the higher energy Fe K feature in Table 1) and we find marginally significant, narrow Fe XXV (f) emission at the galaxy systemic velocity (detected at  $> 95\%$  confidence, since  $\Delta C$  improves by  $\sim 5.6$  for the addition of one free parameter).

### 3.2. Single Relativistic Disk Line Model

TABLE 1. DOUBLE GAUSSIAN MODEL

	Low-Ionization Fe K Peak	High-Ionization Fe K Peak
E(keV)	$6.301^{+0.076}_{-0.073}$	$6.906^{+0.028}_{-0.037}$
$c\Delta E/E_0(\text{km s}^{-1})^a$	$4640^{+3420}_{-3560}$	$2585^{+1590}_{-1210}$
$\sigma(\text{eV})$	$186^{+90}_{-66}$	$36^{+51}_{-24}$
FWHM( $\text{km s}^{-1}$ ) <sup>a</sup>	$20,825^{+10,110}_{-7375}$	$3680^{+5200}_{-2455}$
$I^b$	$19.0^{+8.0}_{-6.9}$	$6.2^{+4.4}_{-3.1}$
EW(eV)	$110^{+46}_{-40}$	$42^{+30}_{-21}$
$\Gamma$	$1.76 \pm 0.06$	...
$\Delta C^c$	-26.1	-10.6
C (d.o.f.) <sup>d</sup>	518.2(508)	...

NOTE. — Model parameters for the best-fitting double-Gaussian model for the double-peaked Fe K complex in the HEG spectrum IC 4329A (see §3.1). Errors are 90% confidence for one interesting parameter ( $\Delta C = 2.706$ ). All parameters are in the source rest frame ( $z = 0.016054$ ). <sup>a</sup> We show *redshift* of the line centroid energy as a velocity offset when the low and high energy peaks are identified with Fe I  $K\alpha$  emission and Fe XXVI  $\text{Ly}\alpha$  respectively. Fe I  $K\alpha$  emission and Fe XXVI  $\text{Ly}\alpha$  emission have rest energies of 6.400keV and 6.966keV respectively. Velocities are rounded to the nearest  $5 \text{ km s}^{-1}$ . Compare these values with the systematic uncertainty in the *HETGS* energy scale of  $\pm 420, \pm 460 \text{ km s}^{-1}$  at the observed energies of the emission peaks. <sup>b</sup> Gaussian emission-line intensity in units of  $10^{-5} \text{ photons cm}^{-2} \text{ s}^{-1}$ . <sup>c</sup> Change in the  $C$ -statistic upon addition of the particular Gaussian model component to a simple power-law model for the continuum (there are three additional degrees of freedom for each Gaussian component). <sup>d</sup> Degrees of freedom.

Next, we replaced the double-Gaussian emission-line model described above with a single, broad emission line model from a relativistic disk around a Schwarzschild black hole (e.g. Fabian *et al.* 1989). These data cannot distinguish between Kerr and Schwarzschild metrics (see §3.6). The inner radius of the disk was fixed at  $6r_g$  since it could not be constrained. The outer disk radius and line intensity were free parameters. The radial line emissivity per unit area was a power law,  $r^q$ , where  $q$  is the emissivity index. This time we also included another disk-line component to model Fe  $K\beta$  emission. Although it makes little difference to the results, we included it for completeness. The rest energy was fixed at 7.056 keV (corresponding to Fe I emission) for simplicity even though the energy of Fe  $K\alpha$  was allowed to vary (but the proximity of the latter energy to the Fe I  $K\alpha$  energy, combined with the relative weakness of  $K\beta$  easily justifies this assumption). The Fe I  $K\beta$  disk-line parameters were coupled to those of the lower energy  $K\alpha$  line, with the intensity of  $K\beta$  tied to (17/150) times the  $K\alpha$  line intensity. There were a total of five free parameters for this emission-line model, including the intrinsic rest energy of the monochromatic emission line. The best-fitting results for this model are given in Table 2 and the data and model are shown in Fig. 4(b). The complex Fe-K emission can clearly be fitted with a single broad line given: a flat radial emissivity ( $q > -0.72$ ) with emission from  $\sim 6$ – $70 r_g$  and  $\theta \sim 24^{+9}_{-1}$  degrees (90%, one-parameter uncertainties). The best-fitting rest-frame energy for this relativistically broadened line is  $6.74^{+0.22}_{-0.13} \text{ keV}$ , which is indicative of He-like Fe. The  $C$ -statistic for the single disk-line model is *higher* (by  $\sim 8.5$ , corresponding to  $> 99\%$  confidence) than that for the double-Gaussian fit in Table 1. However, the single disk-line model we use may be too simplistic (in particular with respect to the assumed simple emissivity law and the assumption of axisymmetric emission), so we cannot rule it out on the basis of the fit statistic alone. Note also that the flat line-emissivity index may be a result of fixing the inner disk radius at  $6r_g$ .

TABLE 2. SINGLE DISK LINE MODEL AND HE-LIKE FE ABSORPTION

	Disk line (No Fe XXV) <sup>a</sup>	Disk Line (With Fe XXV) <sup>b</sup>	Absorption Line
E(keV)	6.74 <sup>+0.22</sup> <sub>-0.13</sub> <sup>c</sup>	6.85 <sup>+0.08</sup> <sub>-0.17</sub>	6.7 (fixed)
$q$	> -0.7	0.6 <sup>+3.3</sup> <sub>-1.7</sub>	...
$\theta(^{\circ})$	24 <sup>+9</sup> <sub>-1</sub>	22 <sup>+7</sup> <sub>-12</sub>	...
$r_{\text{out}}/r_g$	55 <sup>+9</sup> <sub>-9</sub>	48 <sup>+24</sup> <sub>-25</sub>	
FWHM(km s <sup>-1</sup> )	...	...	12, 120 <sup>+11,070</sup> <sub>-6530</sub>
$I$ <sup>d</sup>	23.7 <sup>+7.0</sup> <sub>-6.1</sub>	33.8 <sup>+7.4</sup> <sub>-11.1</sub>	...
EW(eV)	161 <sup>+48</sup> <sub>-44</sub>	249 <sup>+55</sup> <sub>-88</sub>	46 <sup>+22</sup> <sub>-28</sub>
$\Gamma$	1.74 <sup>+0.06</sup> <sub>-0.05</sub>	1.75 <sup>+0.08</sup> <sub>-0.05</sub>	...
$\Delta C$ <sup>e</sup>	32.3	...	...
$C$ (d.o.f.) <sup>f</sup>	526.7 (509)	520.5 (507)	...

NOTE. — Model parameters for the best-fitting relativistic Schwarzschild disk line models (with and without Fe XXV He-like resonance absorption) fitted to the Fe K complex in the HEG spectrum of IC 4329A (see §3.2). All parameters are in the source rest frame ( $z = 0.016054$ ). Errors are 90% confidence for one interesting parameter ( $\Delta C = 2.706$ ). The inner radius of the disk-line model component was fixed at  $6r_g$ . <sup>a</sup> Model fitted with no Fe XXV He-like resonance absorption. <sup>b</sup> Model includes an inverted Gaussian with center energy fixed at 6.7 keV to model Fe XXV He-like resonance absorption (best-fitting absorption-line parameters are given in the last column of the table). <sup>c</sup> There are local minima all the way up to the rest energy of Fe XXVI Ly $\alpha$  (6.966 keV). <sup>d</sup> Fe-K emission-line intensity in units of  $10^{-5}$  photons cm<sup>-2</sup>s<sup>-1</sup>. <sup>e</sup> Change in the  $C$ -statistic upon the addition of the disk-line model component to a simple power-law model. <sup>f</sup> Degrees of freedom.

If the line emission is truncated at a larger radius, a steeper emissivity law is allowed (e.g. see Done *et al.* 2000). When we fixed  $q$  at  $-2.5$  (a value typically found in relativistic Fe K line fits to CCD data) and allowed the inner radius to vary, a fit was obtained which was only marginally worse ( $|\Delta C| < 3$ ), and yielded an inner radius of  $28_{-10}^{+11}r_g$ .

### 3.3. Single Disk Line with Fe XXV He-like Absorption

It is conceivable that between the low-energy and high-energy peaks of the Fe K emission-line complex, we may have Fe XXV He-like resonance absorption at 6.7 keV. Such resonance absorption cutting away the Fe K emission-line profile has been suggested for NGC 3516 (Nandra *et al.* 1999) and MCG -6-30-15 (Fabian *et al.* 2002) and discussed in a theoretical context by, for example, Ruszkowski & Fabian (2002). Therefore, we tested the data against a simple model of Fe XXV He-like resonance absorption by adding an inverted Gaussian component to the single disk-line model described in §3.2. The center energy was fixed at 6.7 keV in the rest frame of the source, which meant that two more free parameters were added to the model (the width and equivalent width of the absorption line). The results for both the relativistic Fe K emission line and the absorption line are shown in Table 2 so that they can be directly compared with the fit with the relativistic Fe K emission line only (§3.2). It can be seen that the addition of the absorption line has little effect on the disk inclination angle, the disk outer radius, and the radial emissivity derived from the broad Fe K line. Naturally, the intensity and equivalent width of the Fe K emission line are required to be larger due to the presence of the absorption line. The derived equivalent width of the absorption line is  $46_{-28}^{+22}$  eV, and its width is  $12, 120_{-6530}^{+11,070}$  km s<sup>-1</sup>. These values depend somewhat on how the underlying emission line is modeled. However, since the addition of the absorption line decreases

the  $C$ -statistic by only 6.2 for the addition of two free parameters (corresponding to a significance of  $< 99\%$ ), we do not pursue the matter further.

### 3.4. Double Disk Line Model

Next, we fit the Fe K emission-line complex with two  $K\alpha$  disk-line model components. The idea here is to investigate in a very simplistic way, the possibility of line emission from a disk with a vertically stratified ionization structure. For example, the higher energy peak could come from a highly ionized top layer, whilst the lower energy line emission could come from a cooler layer beneath the hot layer. Pairs of parameters corresponding to the inclination angle, the inner and outer radii for the two disk-line components were tied so that they were forced to vary together. Both disk-line model components had inner radii fixed at  $6r_g$ . The rest-energy for the lower energy line component was a free parameter but the rest energy of the higher energy line was fixed at the rest-energy of Fe XXVI Ly $\alpha$  (6.966 keV). Thus, the radial line emissivities of the two disk-line components were independent. The above simplifying assumptions are necessary, given the limitations of the data, in order not to over-parameterize the model. Again, for completeness we added an extra disk-line component to model Fe K $\beta$  emission associated with the lower energy peak, as described in §3.2 for the single disk-line model. However, inclusion of the Fe K $\beta$  emission does *not* add any more free parameters to the model. Thus, there were a total of six free parameters in this model of the Fe K emission complex. The best-fitting results for this model are given in Table 3 and the data and model are shown in Fig 4(c). Clearly both disk lines have very similar radial emissivity profiles and are strongly constrained to a near face-on inclination ( $\theta < 6.0^{\circ}$  at  $> 95\%$  confidence). The EWs of the low and high energy features, as modeled by disk lines, are larger than the corresponding EWs in Table 1 (double-Gaussian model) and their combined EW is larger than the single disk-line fit to the Fe K region (at 90% confidence). The fit statistic is an improvement over the double-Gaussian model fit at  $> 95\%$  confidence and is an improvement over the single disk-line model at  $> 3\sigma$  confidence ( $\Delta C = -12.6$  for one additional free parameter).

### 3.5. Relativistic Disk Line and Gaussian Model

Next, we modeled the two peaks in the Fe K band with a relativistic disk line for the lower energy emission component and a Gaussian for the higher energy component. Again, we included Fe K $\beta$  emission as described in §3.2 for completeness. The best-fitting results for this model are given in Table 4. The disk inclination angle is tightly constrained to be  $12 \pm 2$  degrees and  $q$  is flat. The Gaussian best-fitting parameters to the high-energy feature are similar to those in Table 1, as we should expect. This model is not significantly better than the double-Gaussian model statistically (Table 1), but it is better than the single broad disk-line fit (Table 2) at  $> 95\%$  confidence since the  $C$ -statistic decreases by  $\sim 10.3$  for three additional free parameters (relative to the single disk-line model). Note that the radial emissivity power-law index ( $q$ ) for the disk-line emission is very flat.

### 3.6. Complex Continuum

So far, we have not included the effects of a Compton-reflection continuum, or indeed any other complexity in the continuum. First of all, we note that there is little evidence

TABLE 3. DOUBLE DISK-LINE MODEL

	Low-ionization Fe K	Fe XXVI Ly $\alpha$
E(keV)	6.443 <sup>+0.050</sup> <sub>-0.016</sub>	6.966 fixed
$q^a$	-2.44 <sup>+0.22</sup> <sub>-0.24</sub>	-2.20 <sup>+0.33</sup> <sub>-0.37</sub>
$\theta(^{\circ})^b$	< 6.0	...
$r_{\text{out}}/r_g^b$	633 <sup>+57</sup> <sub>-369</sub>	...
$I^c$	20.6 <sup>+6.4</sup> <sub>-6.7</sub>	14.5 <sup>+6.3</sup> <sub>-7.0</sub>
EW(eV)	120 <sup>+37</sup> <sub>-36</sub>	101 <sup>+44</sup> <sub>-49</sub>
$\Gamma$	1.79 <sup>+0.06</sup> <sub>-0.05</sub>	...
$\Delta C^d$	-25.2	-22.9
$C$ (d.o.f.) <sup>e</sup>	514.1 (507)	...

NOTE. — Parameters for the best-fitting double relativistic disk-line fit to the Fe K line region of the HEG spectrum in IC 4329A. The model includes an Fe K  $\beta$  emission component for the lower-energy line (see §3.4 for fitting details). Errors are 90% confidence for one interesting parameter ( $\Delta C = 2.706$ ) except where noted. The inner radius of all disk-line model components was fixed at  $6r_g$ . All parameters are in the source rest frame ( $z = 0.016054$ ). The energy of the Fe XXVI Ly $\alpha$  disk line component was fixed at its rest energy of 6.966 keV. <sup>a</sup> Power-law index for the line radial emissivity. The lower energy Fe K $\alpha$  and Fe XXVI Ly $\alpha$  disk line components were coupled in all parameters except this one ( $q$ ). <sup>b</sup> Both  $\theta$  and  $r_{\text{out}}/r_g$  for the Fe XXVI Ly $\alpha$  disk line were forced to their corresponding values for the lower energy disk line during the fitting. The  $C$ -statistic varies non-monotonically close to the best fit. For the disk inclination angle the 95% confidence upper limit is shown. Formally,  $\theta < 0.35^{\circ}$  at 90% confidence but the 95% confidence value is more reliable since it is in the region where  $C$  is well-behaved. For  $r_{\text{out}}/r_g$ , the errors represent 90% confidence values, but only when  $\Delta C$  never drops below 2.706 again. <sup>c</sup> Line intensity in units of  $10^{-5}$  photons  $\text{cm}^{-2}\text{s}^{-1}$ . <sup>d</sup> Change in  $C$ -statistic upon the addition of the particular disk line model component to a power-law continuum only. <sup>e</sup> Degrees of freedom.

of an Fe K edge above 7 keV in the data (Fig. 4). An Fe K edge could be produced either in transmission or reflection from optically-thick matter. We added a simple edge model to the disk-line plus Gaussian model (§3.5), at 7.11 keV (corresponding to neutral Fe) and found a best-fit value of zero, and a 90%, one-parameter upper limit of  $\tau_{\text{Fe}} < 0.054$ . This is comparable with  $\tau_{\text{Fe}} \sim 0.03$  from the *XMM-Newton* observation of IC 4329A by Gondoin *et al.* (2001). This implies a total neutral absorbing column of  $N_H < 4.9 \times 10^{22} \text{ cm}^{-2}$  in the line-of-sight. This is certainly consistent with the low-energy MEG data (McKernan, Yaqoob, & Reynolds 2004, in preparation).

Due to the restricted bandpass and limited signal-to-noise, the data are not sensitive to the Compton-reflection continuum, which becomes important above  $\sim 7$  keV. However, we demonstrated this directly by fitting a model consisting of a power law with a high-energy exponential cut-off, and Compton reflection from optically-thick, neutral matter (using the XSPEC model `pe xrav`, as described in Magdziarz & Zdziarski 1995), a Fe K $\alpha$  line to model the lower energy peak in the Fe complex, and another emission line to model the higher energy peak. A Fe K $\beta$  line was also included, for completeness, and tied to the Fe K $\alpha$  line as described in §3.2. The Fe K $\alpha$  line, the Fe K $\beta$  line, and the Compton reflection continuum were all blurred with a relativistic kernel based on the Kerr metric (Laor 1991; see also Fabian *et al.* 2002). The reason for now using the Kerr metric (for a maximally spinning black hole), instead of the Schwarzschild metric, is to directly demonstrate that the data are not sensitive to the black-hole angular momentum. Since the higher energy peak of the Fe complex (possibly due to Fe XXVI Ly $\alpha$ ) in the IC 4329A HEG data is quite narrow, it was modeled with a Gaussian and *not* subjected to the relativistic blurring. Also, we included no Compton-reflection continuum associated with the the higher

TABLE 4. DISK LINE PLUS GAUSSIAN LINE MODELS

	Disk Line (simple) <sup>a</sup>	Gaussian (simple) <sup>a</sup>	Disk Line (complex) <sup>b</sup>	Gaussian (complex) <sup>b</sup>
E(keV)	6.412 <sup>+0.045</sup> <sub>-0.027</sub>	6.900 <sup>+0.036</sup> <sub>-0.030</sub>	6.349 <sup>+0.262</sup> <sub>-0.071</sub>	6.900 <sup>+0.036</sup> <sub>-0.030</sub>
$q$	-0.37 <sup>+2.50</sup> <sub>-1.08</sub>	...	> -2.4	...
$\theta(^{\circ})$	12 $\pm$ 2	...	18 <sup>+7</sup> <sub>-16</sub>	...
$r_{\text{out}}/r_g$	105 <sup>+31</sup> <sub>-79</sub>	...	> 13	...
$c\Delta E/E_0(\text{km s}^{-1})^c$	...	2840 <sup>+1295</sup> <sub>-1550</sub>	...	2840 <sup>+1295</sup> <sub>-1550</sub>
$\sigma(\text{eV})$	...	46 <sup>+36</sup> <sub>-31</sub>	...	40 <sup>+41</sup> <sub>-27</sub>
FWHM(km s <sup>-1</sup> ) <sup>c</sup>	...	4710 <sup>+3680</sup> <sub>-3175</sub>	...	4095 <sup>+4195</sup> <sub>-2765</sub>
$I^d$	16.1 <sup>+5.0</sup> <sub>-4.8</sub>	5.4 <sup>+5.1</sup> <sub>-3.2</sub>	15.9 <sup>+13.7</sup> <sub>-6.9</sub>	6.0 <sup>+3.3</sup> <sub>-2.9</sub>
EW (eV)	96 <sup>+30</sup> <sub>-29</sub>	36 <sup>+34</sup> <sub>-21</sub>	88 <sup>+76</sup> <sub>-38</sub>	40 <sup>+22</sup> <sub>-21</sub>
$\Gamma$	1.75 $\pm$ 0.05	...	1.87 <sup>+0.20</sup> <sub>-0.17</sub>	...
$R^e$	...	...	< 2.9	...
$\Delta C$	-30.2 <sup>h</sup>	-12.2 <sup>h</sup>	-32.6 <sup>g</sup>	-9.6 <sup>h</sup>
$C$ (d.o.f.) <sup>f</sup>	516.4 (506)	...	516.8(505)	...

NOTE. — Model parameters for the best-fitting relativistic disk line plus Gaussian models to the Fe K complex in the HEG spectrum of IC 4329A (see §3.5 for fitting details). The model also includes Fe K  $\beta$  emission for the lower energy line (see §3.2 for details). Errors are 90% confidence for one interesting parameter ( $\Delta C = 2.706$ ). The inner radius of the lower energy Fe K $\alpha$  disk-line model was fixed at  $6r_g$ . All quantities are quoted in the source rest frame ( $z = 0.016054$ ). <sup>a</sup> Simple model with a power-law continuum, and a relativistic disk line for a Schwarzschild black-hole. <sup>b</sup> Relativistic disk line from maximally rotating Kerr black-hole, with a power-law plus Compton-reflection continuum blurred by the relativistic line kernel. Fe XXVI Ly $\alpha$  has a rest energy of 6.966 keV. <sup>c</sup> Velocities are rounded to nearest 5  $\text{km s}^{-1}$ . <sup>d</sup> Line intensity in units of  $10^{-5}$  photons  $\text{cm}^{-2}\text{s}^{-1}$ . <sup>e</sup> Effective ‘reflection fraction’ (i.e.  $R = 1$  corresponds to the steady-state Compton reflection amplitude from an infinite disk subtending  $2\pi$  solid angle at the X-ray source). <sup>f</sup> Degrees of freedom. <sup>g</sup> Change in the  $C$ -statistic upon addition of only the disk line to the continuum. <sup>h</sup> Change in the  $C$ -statistic upon addition of a Gaussian emission-line component to the disk-line plus continuum model.

energy peak. This is because if it is due to highly ionized Fe, the curvature in the reflected continuum is much less than the case for a disk which is not ionized, especially for data in the restricted bandpass (3–8 keV) that we are dealing with here. If the higher energy feature is not a separate line, then the single Compton-reflection continuum already included is adequate.

The free parameters of the `laor` model were the disk inclination angle,  $\theta$ , the power-law emissivity index,  $q$ , and the outer disk radius,  $r_{\text{out}}$ . Since even the lower energy emission peak is not extremely broad, we found the fit to be quite insensitive to the inner disk radius, so again fixed it at  $6r_g$ . The Compton-reflection model (`pe xrav`) does not allow the disk inclination angle to be tied to that of the `laor` model, and also does not allow inclination angles  $< 18^{\circ}$ . Therefore we fixed the inclination angle at  $30^{\circ}$  for the Compton-reflection continuum. This is adequate for our purpose. We also assumed solar element abundances and an exponential cut-off energy of 200 keV for the intrinsic power-law continuum. This is consistent with broadband observations of IC 4329A as well as results for other AGNs (e.g. Madejski *et al.* 1995; Malizia *et al.* 2003; Perola *et al.* 2002). In any case, our conclusions are not sensitive to this assumption. The Compton-reflection continuum then had only one free parameter in the fit, the ratio,  $R$ , of the amplitude of the reflected continuum to that expected from a centrally illuminated infinite disk, subtending a solid angle of  $2\pi$  at the X-ray source. In all, this model had eleven free parameters, including the overall continuum normalization. This is one more free parameter than the equivalent model that utilized the Schwarzschild metric and that did not include a Compton-reflection continuum (i.e. the model described in §3.5).

The results are shown in Table 4 so that they can be directly compared with the results when Compton reflection was not included, and the continuum was modeled only with a simple power law. It can be seen that the quality of the fits for the two models, the best-fitting values for the emission-line parameters and their statistical error ranges are virtually indistinguishable. This applies to both the relativistic and non-relativistic emission lines. It is important to note, however, that inclusion of the Compton-reflection continuum does allow the line radial emissivity index to be steeper, relieving the requirement that the emissivity law be flat (which may be physically difficult to achieve). Another noticeable difference between the simple and complex continuum fits is that the latter fit yields a somewhat steeper intrinsic X-ray continuum power-law index. For the fit with a complex continuum, the reflection fraction,  $R$ , was consistent with zero, and we obtained an upper limit of  $R < 2.9$  (90% confidence, one parameter). This confirms that the data are insensitive to the Compton-reflection continuum. The result also justifies using only a simple power-law for the continuum in the model-fitting described in §3.1 – §3.5. Since the relativistically smeared Compton-reflection continuum is smoother and produces less curvature in the net spectrum than an unsmeared continuum (in the energy band relevant here), we tested the data against the same model with the smearing of the Compton-reflection component turned off. Physically, such a component could originate in optically-thick distant matter, such as a parsec-scale torus. Again, no reflection was formally required by the data, with a 90% confidence upper limit of  $R < 1.7$ . These results further justify using only a simple power law for the continuum in the model-fitting described in §3.1 – §3.5.

#### 4. DISCUSSION

In a *Chandra* HETGS observation of IC 4329A, we have measured broad and complex line emission in the Fe K band using the highest spectral resolution currently available in the Fe K band ( $\sim 1860$  km s<sup>-1</sup> FWHM at 6.4 keV). The line profile is double-peaked, the peaks occurring at  $\sim 6.3$  keV and  $\sim 6.9$  keV in the source rest frame. Modeled with Gaussians, the lower and higher energy peaks have widths of  $20,825^{+10,110}_{-7,375}$  km s<sup>-1</sup> FWHM and  $3680^{+5200}_{-2455}$  km s<sup>-1</sup> FWHM respectively. The lower energy peak is resolved by the high energy grating (HEG) at  $> 99\%$  confidence, whilst the higher energy peak is only resolved at  $< 90\%$  confidence. The low-energy peak is redshifted from the expected rest-frame energy of Fe I K $\alpha$  by at least  $650$  km s<sup>-1</sup> and the high-energy peak is redshifted from the expected rest-frame energy of Fe XXVI Ly $\alpha$  by at least  $950$  km s<sup>-1</sup>. Both of these lower limits on the redshift correspond to 90% confidence levels for one parameter. The emission-line peak at  $\sim 6.9$  keV that we found in the *Chandra* HETGS data has not been detected in any previous observations of IC 4329A. We also detected a much weaker emission peak at the expected energy of the Fe XXV forbidden line energy at the systemic velocity of IC 4329A, but the feature is detected only with a marginal significance ( $> 95\%$  confidence).

The amount of Fe in the line-of-sight may be insufficient to produce all of the observed EW of the lower energy  $\sim 6.3$  keV Fe K feature ( $110^{+46}_{-40}$  eV from Table 1) since the measured (HEG) upper limit on the optical depth of an Fe K edge corresponds to an absorbing column density  $< 4.9 \times 10^{22}$  cm<sup>-2</sup> and this is consistent with the low-energy MEG data from the same observation (McKernan, Yaqoob & Reynolds 2004 in

preparation; see also Gondoin *et al.* 2001). Such a column density can at most produce an EW of  $< 50$  eV, even if it fully covered the sky (e.g. Krolik & Kallman, 1987; Yaqoob *et al.* 2001). To investigate the contribution to the Fe K line emission from distant matter, we added an extra (narrow) Gaussian line component to the two Gaussian model described in Table 1. The energy of the new Gaussian component was fixed at 6.4 keV in the rest-frame of the AGN since we are testing the data for a line which originates from matter sufficiently distant that there is no gravitational redshift. Also, a line originating from such distant matter would be unresolved by *Chandra*, so we fixed the width of the Gaussian at a value (1 eV) much less than the instrument resolution. The two other Gaussian model components were allowed to vary as before. The best-fitting model did not result in a significant improvement in the fit-statistic ( $\Delta C = 2.3$  for one additional free parameter). Thus, the values and error ranges of all the model parameters did not change significantly compared to the values shown in Table 1, which were obtained without the distant-matter line. The 90% confidence (one-parameter) upper limit on the distant-matter line EW we obtained is 18 eV, so that it could contribute at most  $\sim 1/4$  of the low energy (6.2–6.4 keV) Fe K line emission in IC 4329A. This and the fact that the low-energy peak is at 6.3 keV and resolved by the HEG suggests that the contribution from distant matter is not as important as in some other AGN in which the Fe K line emission peaks at 6.4 keV and is unresolved by the HEG (see Yaqoob & Padmanabhan 2004). Thus, it is likely that the bulk of the  $\sim 6.3$  keV line emission originates in an accretion disk. It is difficult to deduce what the ionization state of the matter must be because of the possibility of a peak at energies higher than 6.4 keV being gravitationally redshifted down to  $\sim 6.3$  keV. Note that a radius of  $\sim 65r_g$  is required to gravitationally redshift a 6.4 keV line to 6.3 keV.

The interpretation of the overall, double-peaked Fe K line profile is difficult. Several physically distinct models can describe the data. The two peaks may correspond to the Doppler horns of a single disk line or they may be artificial in the sense that He-like Fe K absorption has removed the central portion of a disk line profile which may not have prominent Doppler peaks. Alternatively, the higher energy peak at 6.9 keV may correspond to Fe XXVI Ly $\alpha$  emission which is independent of the line emission associated with the lower energy peak. In that case, the Fe XXVI Ly $\alpha$  line may or may not originate in a disk. Again the two scenarios are degenerate as far as the data are concerned. If there is Fe XXVI Ly $\alpha$  line emission from a disk it may come from a layer which is hotter than that producing the lower-energy line (for example the hot corona, e.g. see Nayakshin & Kallman 2001; Ballantyne, Ross, & Fabian 2001). Although the  $\sim 6.9$  keV line appears to be fairly narrow we have shown by direct model fitting that it could still originate from a disk which extends down to  $6r_g$ , with a radial line emissivity per unit area which is *not* flat.

The line emission peak at 6.9 keV is reminiscent of a similar feature found in a long *XMM-Newton* exposure of the Seyfert galaxy MCG -6-30-15 (e.g. Fabian *et al.* 2002). In that case there is also an ambiguity between Fe XXV He-like absorption and Fe XXVI Ly $\alpha$  emission, and the peak energy is slightly redshifted from the expected energy of Fe XXVI Ly $\alpha$ , just as in IC 4329A. Fe XXV He-like absorption has actually been observed with less ambiguity in some AGN (PG 1211+143, Pounds *et al.* 2003a; PG 0844+349, Pounds *et al.* 2003b; NGC 3783, Reeves *et al.* 2003).

Although there are several interpretations of the complex

Fe K emission revealed by the HEG spectrum of IC 4329A, each of the different scenarios is interesting from the point of view that future observations with *Astro-E2* will break much of the degeneracy and whichever scenario turns out to be correct, we would learn something new about the central engine. In particular, observational constraints on the ionization structure of the accretion disk in AGN are currently very poor and IC 4329A may be a good astrophysical laboratory for improving them.

We gratefully acknowledge support from NSF grant

AST0205990 (BM) and NASA grants NCC5-447 (TY) and NAG5-10769 (TY). We thank A. C. Fabian for providing us with a relativistic blurring routine. We also thank Urmila Padmanabhan for help with some of the data analysis. We made use of the HEASARC on-line data archive services, supported by NASA/GSFC and also of the NASA/IPAC Extragalactic Database (NED) which is operated by the Jet Propulsion Laboratory, California Institute of Technology, under contract with NASA. We are grateful to the *Chandra* instrument and operations teams for making this observation possible.

#### REFERENCES

- Ballantyne, D., Ross, R. R., & Fabian, A. C. 2001, MNRAS, 327, 10  
 Ballantyne, D., & Ross, R. R. 2002, MNRAS, 333, 777  
 Bautista, M. A., Kallman, T. R., Angelini, L., Liedahl, D. A., & Smits, D. P. 1998, ApJ, 509, 848  
 Bautista, M. A., & Titarchuk, L. 1999, ApJ, 511, 105  
 Cappi, M., Mihara, T., Matsuoka, M., Hayashida, K., Weaver, K. A., & Otani, C., 1996, ApJ, 458, 149  
 Cash, W., 1976, A&A, 52, 307  
 Comastri, A., *et al.* 1998, A&A, 331, 31  
 Dewangan, G. C. 2002, ApJ, 581, L71  
 Done, C., Madejski, G. M., & Zycki, P. T. 2000, ApJ, 536, 213  
 Elvis, M. 2000, ApJ, 545, 63  
 Elvis, M., Wilkes, B. J., & Lockman, F. J. 1989, AJ, 97, 777  
 Fabian, A. C., Rees, M. J., Stella, L., & White, N. E. 1989, MNRAS, 238, 729  
 Fabian, A. C., Iwasawa, K., Reynolds, C. S., & Young, A. J. 2000, PASP, 112, 1145  
 Fabian, A. C., *et al.* 2002, MNRAS, 335, L1  
 Fang, T., Davis, D. S., Lee, J. C., Marshall, H. L., Bryan, G. L., & Canizares, C. R. 2002, ApJ, 565, 86  
 Gondoin, P., Barr, P., Lumb, D., Oosterbroek, T., Orr, A., & Parmar, A. N. 2001, A&A, 378, 806  
 Hartnoll, S. A. & Blackman, E. G., 2000, MNRAS, 317, 880  
 Kaspi, S., *et al.* 2002, ApJ, 554, 216  
 Krolik, J. H., & Kallman, T. 1987, ApJ, 320 L5  
 Laor, A., 1991, ApJ, 376, 90L  
 Lee, J. C., Reynolds, C. S., Remillard, R., Schulz, N. S., Blackman, E. G., & Fabian, A. C. 2002, ApJ, 567, 1102  
 Lubiński, P., & Zdziarski, A. A. 2001, MNRAS, 323, L37  
 Madejski, G. M., *et al.* 1995, ApJ, 438, 672  
 Magdziarz, P., & Zdziarski, A. A. 1995, MNRAS, 273, 837  
 Malizia, A., Bassani, L., Stephen, J. B., Di Cocco, G., Fiore, F., & Dean, A. J. 2003, ApJ, 589, L17  
 Markert, T. H., Canizares, C. R., Dewey, D., McGuirk, M., Pak, C., & Shattenburg, M. L. 1995, Proc. SPIE, 2280, 168  
 Muzhotzky, R. F., Fabian, A. C., Iwasawa, K., Kunieda, H., Matsuoka, M., Nandra, K., & Tanaka, Y., 1995, MNRAS, 272, L9  
 Nandra, K., George, I. M., Turner, T. J., & Fukazawa, Y. 1996, ApJ, 464, 165  
 Nandra, K., George, I. M., Mushotzky, R. F., Turner, T. J., & Yaqoob, T. 1997, ApJ, 476, 70  
 Nandra, K., George, I. M., Mushotzky, R. F., Turner, T. J., & Yaqoob, T. 1999, ApJ, 523, L17  
 Nayakshin, S., & Kallman, T., 2001, ApJ, 546, 406  
 Page, M. J., Davis, S. W., & Salvi, N. J. 2003, MNRAS, 343, 1241  
 Perola, G. C., *et al.* 1999, A&A, 351, 937  
 Perola, G. C., Matt, G., Cappi, M., Fiore, F., Guainazzi, M., Maraschi, L., Petrucci, P. O., & Piro, L. 2002, A&A, 389, 802  
 Petrucci, P. O., *et al.* 2002, A&A, 388, L5  
 Pounds, K. A., Reeves, J. N., O'Brien, P. T., Turner, M. J. L., & Nayakshin, S. 2001, ApJ, 559, 181  
 Pounds, K. A., Reeves, J. N., King, A. R., Page, K. L., O'Brien, P. T., & Turner, M. J. L. 2003a, MNRAS, 345, 705  
 Pounds, K. A., King, A. R., Page, K. L. & O'Brien, P. T. 2003b, MNRAS, 346, 1025  
 Reeves, J. N. in Proc. 'Active Galactic Nuclei: from Central Engine to Host Galaxy', Meudon, July 2002 meeting; ASP Conference Series, Eds.: S. Collin, F. Combes, & I. Shlosman  
 Reeves, J. N., Nandra, K., George, I. M., Pounds, K. A., Turner, T. J. & Yaqoob, T., ApJ(accepted), astro-ph/0310820  
 Reynolds, C. S. 1997, MNRAS, 286, 513  
 Reynolds, C. S., Ward, M. J., Fabian, A. C., & Celotti, A. 1997, MNRAS, 291, 403  
 Reynolds, C. S., & Nowak, M. A., 2003, Phys. Rep., 377, 389  
 Ruszkowski, M., & Fabian, A. C. 2000, MNRAS, 315, 223  
 Spergel, D. N., *et al.* 2003, ApJS, 148, 175  
 Sulentic, J. W., Marziani, P., Zwitter, T., Calvani, M., & Dultzin-Hacyan, D. 1998, ApJ, 501, 54  
 Turner, T. J., George, I. M., & Nandra, K. 1998, ApJ, 508, 2  
 Turner, T. J., George, I. M., Nandra, K., & Turcan, D. 1999, ApJ, 524, 667  
 Turner, T. J., *et al.* 2002, ApJ, 574, L123  
 Ward, M., Elvis, M., Fabbiano, N., Carleton, P., Willner, S. P., & Lawrence, A. 1987, ApJ, 315, 74  
 Willmer, C. N. A., Focardi, P., Chan, R., Pilligrini, P. S., & Nicolaci da Costa, L. 1991, AJ, 101, 57  
 Yaqoob, T., George, I. M., Nandra, K., Turner, T. J., Serlemitsos, P. J., & Mushotzky, R. F. 2001, ApJ, 546, 759  
 Yaqoob, T., George, I. M., Kallman, T. R., Padmanabhan, U., Weaver, K. A., & Turner, T. J., 2003a, ApJ, 596, 85  
 Yaqoob, T., McKernan, B., Kraemer, S. B., Crenshaw, D. M., Gabel, J. R., George, I. M., & Turner, T. J., 2003b, ApJ, 582, 105  
 Yaqoob, T., & Padmanabhan, U. 2004, ApJ, in press (astro-ph/0311551)  
 Yaqoob, T., Padmanabhan, U., Dotani, T., & Nandra, K. 2002, ApJ, 589, 487